

The relativistic Iron $K\alpha$ line from an accretion disc onto a static non-baryonic compact object

Youjun Lu^{a*} and Diego F. Torres^b

^aCenter for Astrophysics, University of Sci. & Technology of China, Hefei, Anhui 230026, P. R. China

^bPhysics Department, Princeton University, NJ 08544, USA

November 9, 2018

Abstract

This paper continues the study of the properties of an accretion disc rotating around a non-baryonic (assumed super-massive) compact object. This kind of objects, generically known as boson stars, were earlier proposed as a possible alternative scenario to the existence of super-massive black holes in the center of every galaxy. A dilute boson star has also been proposed as a large part of the non-baryonic dark matter, flattening galactic rotational velocities curves. In this contribution, we compute the profile of the emission lines of Iron; its shape has been for long known as a useful diagnosis of the space-time geometry. We compare with the case of a Schwarzschild black hole, concluding that the differences are observationally distinguishable.

PACS Number(s): 04.40.Dg, 98.62.Mw, 04.70.-s

1 Introduction

It has long been believed that accretion onto massive black holes is the energy source of active galactic nuclei (AGN). Nearby galaxies, as the remnants of AGNs, should then harbor massive black holes in their centers [1]. Recent observations have indeed revealed the existence of massive dark objects, believed to be those massive black holes, in most, if not all, nearby galactic nuclei [2, 3]. However, those observations only reach a physical radius 10000 times larger than that of the event horizon of the putative black hole. As pointed out in Ref. [4], from a dynamical point of view, a single massive boson star is also compatible with all measurements of star kinematics around the massive dark object in the most studied center, that of Milky Way, without requiring the massive dark object to be a black hole. A proof of the existence of massive black holes requires unambiguous evidence of the event horizon. It is then important to address the issue of the emissivity properties of matter rotating around different central objects. Ref. [5] made a first step in this sense; to that paper we refer the reader for further discussions and a more complete list of references on boson star physics and related problems. The emissivity properties are much more important than the kinematic studies, since they can provide a more direct way to actually distinguish between different central objects [6].

X-ray studies have revealed the most prominent spectral feature coming from the central regions of some active galaxies, an enormous Doppler and gravitational-shifted broad Fe $K\alpha$ line, which, for the first time, showed the existence of a strong gravity regime [7, 8]. This has been taken as the strongest evidence

*Current Address: Astrophysical Sciences Department, Princeton University, NJ 08544, USA

for the existence of super-massive black holes, or even as a sensitive diagnosis of the black hole spin. But, how would the profile of the emission lines be for those produced in discs rotating around putative boson stars? Would they present sufficiently different shapes as to make them distinguishable in forthcoming observations? These are the questions we address in this paper.

2 Photon propagation in the metric of a boson star

2.1 Space-time

The space-time generated by a stationary and spherically symmetric object can be described by the metric:

$$ds^2 = B(r)dt^2 - A(r)dr^2 - r^2(d\theta^2 + \sin^2\theta d\phi^2), \quad (1)$$

where $A(r)$ can be written as $1/(1 - 2GM(r)/rc^2)$, c is the speed of light, G is the gravitation constant and $M(r)$ is the mass enclosed within a radius r . The simplest solution for Eq. (1) is that representing a Schwarzschild black hole, for which $B(r) = 1 - 2GM/rc^2$, and $M(r)$ is a constant equal to the mass of the black hole.

Other stellar-like systems described by Eq. (1) are those known as boson stars. Details of boson star solutions can be found in the reviews quoted in Ref. [9]. For a boson star, $A(r)$ and $B(r)$ can be calculated only numerically (see [4] for explanations, the program herein used is an adaptation of that mentioned in Refs. [10]).

The total mass, the radius and all other physical parameters of the boson star are scaled by the mass of the constituent boson, m . For numerical purposes, then, we can work with dimensionless units. The radius in a dimensionless form will be $x = mr$, and the mass, as well, will be transformed into a dimensionless quantity, $M = M(x)M_{\text{Planck}}^2/m$, where $M_{\text{Planck}} = \sqrt{\hbar c/G}$, \hbar is the Planck constant. This scheme was already proposed in the first papers on boson stars [11, 12, 13]. For example, if the massive dark object with mass $2.6 \times 10^6 M_{\odot}$ in the Galactic Center is a boson star, then the constituent boson mass is $m = 2.81 \times 10^{-26}$ GeV. The distance from the center in unit of parsec is $r[\text{pc}] = x/m[\text{GeV}] 6.38 \times 10^{-33}$, the mass in millions of solar mass is $M[10^6] = M(x)/m[\text{GeV}] 1.33 \times 10^{-25}$, and the gravitational radius $r_g = GM/c^2$ is written as $x_g = 0.53256$ in dimensionless units. The boson star structure is numerically computed to obtain $M(x)$ and $B(x)$ [4]. Two notes are, however, in order. Firstly, these numbers rely in that we are using a non self-interacting boson star, for simplicity and because the behavior is generic, but should be consistently changed if this is not the case [4]. By going towards a self-interacting model, the mass of the constituent boson needed to produce the same overall mass increases. Secondly, the use of the mass of the galactic center region is done just to provide a numerical example, we are not claiming the possible existence of a boson star in the center of the Galaxy, since apparently the emissivity properties would conflict with observations (see Ref. [5]), or at least we know that that is the case for the simplest accretion disc models.

To conveniently compare the metric generated by a non-rotating boson star with the Schwarzschild black hole metric, we re-scale the total mass of the boson star to be $M = 1$. We do so by just dividing $x/0.53256$ and replacing $M(x)$ by $M(x)/0.53256$. Figure 1 shows $B(r)$ as a function of r for both boson star and Schwarzschild black hole. $B(r)$ for both cases are almost exactly the same when $r > 15r_g$, while it slowly decreases to a constant at the center of a boson star rather than rapidly decrease to zero at the horizon ($r = 2r_g$) of a Schwarzschild black hole. To a distant observer, thus, a photon emitted from the inner region of a disc extending within a boson star ($r < 15r_g$) suffers much less gravitational redshift than

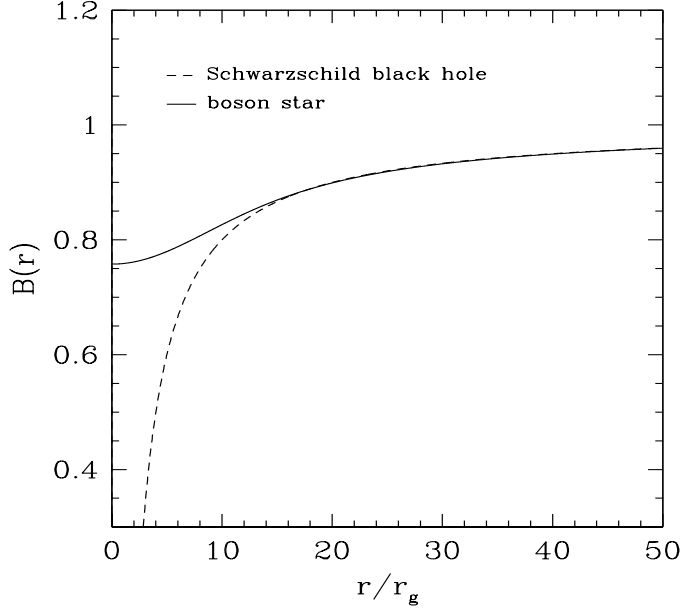


Figure 1: The metric parameter $B(r)$ as a function a radius (in unit of the gravitation radius $r_g = GM/c^2$). The solid line represents a boson star and the dash line represents a Schwarzschild black hole of equal mass. The main difference appears in the inner region, with $r < 15r_g$.

the one emitted from the disc surrounding a Schwarzschild black hole.

To simplify the following calculations, we adopt a simple Logistic function to fit both $M(x)$ and $B(x)$ for $x < 50$,

$$M(x)[\text{or } B(x)] = \frac{A_1 - A_2}{1 + (\frac{x}{x_0})^p} + A_2. \quad (2)$$

For the mass $M(x)$, the coefficients are $A_1 = 0.01039$, $A_2 = 0.53533$, $x_0 = 5.49809$ and $p = 3.6201$; while for $B(x)$ the coefficients are $A_1 = 0.78236$, $A_2 = 0.99793$, $x_0 = 8.17558$ and $p = 2.09499$. Both fits are excellent ($\chi^2 < 10^{-5}$) and valid throughout all space-time (see Fig 2); they much improve those presented in Ref. [4]. For $x > 50$, $M(x)$ and $B(x)$ are almost exactly the same as those obtained in the Schwarzschild black hole case, i.e. $M(x) = 0.53256$ and $B(x) = 1 - 2M(x)/x$.

2.2 Orbits

The Lagrangian of the geodesics in the space-time with a line element shown by Eq. (1) can be written as (cf. [14], pages 342-347 — [15], pages 897-902):

$$2\mathcal{L} = B(r)\dot{t}^2 - A(r)\dot{r}^2 - r^2(\dot{\theta}^2 + \sin^2\theta\dot{\phi}^2), \quad (3)$$

where the dot denotes differentiation with respect to an affine parameter λ along the geodesics. Together with the assumption of stationary and axisymmetric space-time, the Euler-Lagrange equations give the simplified photon momentum equations as (see analogous derivations of the momentum equations for black hole metric in Ref. [14, 15], pages as above):

$$\frac{dt}{d\lambda} = \frac{r^2}{B(r)} \frac{1}{\sqrt{R}}, \quad (4)$$

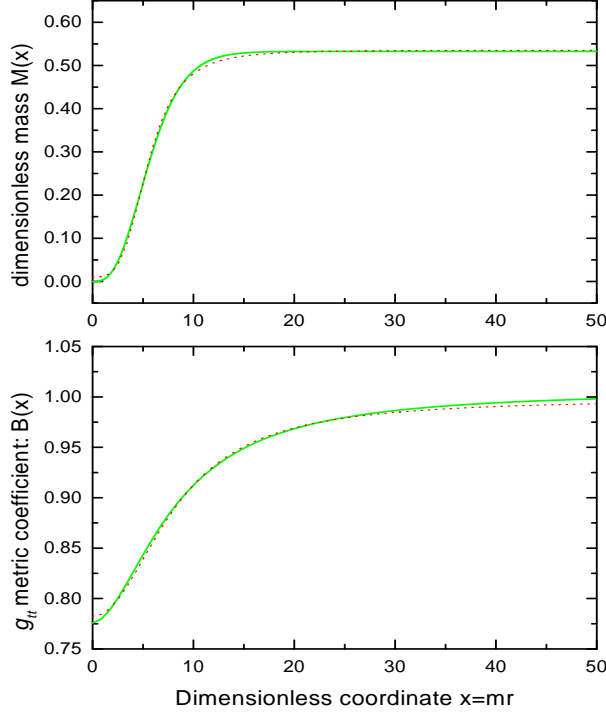


Figure 2: Logistic function fits to both, $B(x)$ and the mass. The fit is actually superposed to the numerical curves in both cases.

$$\frac{dr}{d\lambda} = \pm \frac{\sqrt{R}}{r^2}, \quad (5)$$

$$\frac{d\theta}{d\lambda} = \pm \frac{\sqrt{\Theta}}{r^2}, \quad (6)$$

$$\frac{d\phi}{d\lambda} = \frac{\xi}{r^2 \sin^2 \theta}, \quad (7)$$

where the functions Θ and R are respectively given by

$$\Theta = \eta - \xi^2 \cot^2 \theta, \quad (8)$$

$$R = \frac{r^4}{A(r)B(r)} - \frac{r^2}{A(r)}(\eta + \xi^2), \quad (9)$$

and where $\eta = \mathcal{K}/E^2$ and $\xi = L/E$ are constants of motion related to the angular momentum L , the energy at infinity E , and the Carter's constant $\mathcal{K} = p_\theta^2 + L^2 \cot^2 \theta$. p_θ is the θ -component of photon momentum (cf. the photon momentum equations in the space-time of a Kerr black hole [14, 15], pages as above).

The path of a particular photon is completely described by the motion constants η and ξ , which are in fact related to the polar and azimuthal angles α and β on the sky as seen by a distant, locally non-rotating,

observer who receives the photon. The motion constants η and ξ are then given by ¹

$$\xi = \left(\frac{r \sin \theta \sin \alpha \sin \beta}{\sqrt{B(r)}} \right)_{\theta=\theta_o}, \quad (10)$$

$$\eta = \frac{r^2}{B(r)} \sin^2 \alpha \left(1 - \sin^2 \theta \sin^2 \beta \right)_{\theta=\theta_o}. \quad (11)$$

The equation governing the projection of a photon orbit in (r, θ) plane is

$$\int_{r_i}^r \frac{dr}{\sqrt{R}} = \pm \int_{\theta_i}^{\theta} \frac{d\theta}{\sqrt{\Theta}}, \quad (12)$$

where r_i and θ_i are the initial values of r and θ . The θ -integration, i.e. the right hand of Eq. (12), gives

$$\int \frac{d\theta}{\sqrt{\Theta}} = \frac{1}{\sqrt{\eta + \xi^2}} \cos^{-1} \left(\sqrt{\frac{\eta + \xi^2}{\eta}} \cos \theta \right). \quad (13)$$

The integral for t and ϕ can be written as

$$t = \int \frac{r^2 dr}{B(r) \sqrt{R}}, \quad (14)$$

$$\phi = \int \frac{\xi}{\sin^2 \theta} \frac{d\theta}{\sqrt{\Theta}} = \tan^{-1} \left[\sqrt{\frac{1+K}{1-K}} \tan \left(\frac{\theta'}{2} \right) \right] + \tan^{-1} \left[\sqrt{\frac{1-K}{1+K}} \tan \left(\frac{\theta'}{2} \right) \right], \quad (15)$$

where $K = \sqrt{\frac{\eta}{\eta + \xi^2}}$, and $\theta' = \cos^{-1}(\cos \theta / K)$.

To enable the integration of a given photon away from the observer to the disc surface, it is necessary to determine the initial sign of $dr/d\lambda$ and $d\theta/d\lambda$ which are in fact given by (see Fig. 1a in Ref. [16]):

$$\frac{dr}{d\lambda} > 0 \quad \text{for} \quad 0 \leq \alpha < \pi/2, \quad (16)$$

$$\frac{dr}{d\lambda} < 0 \quad \text{for} \quad \pi/2 \leq \alpha < \pi, \quad (17)$$

$$\frac{d\theta}{d\lambda} > 0 \quad \text{for} \quad |\beta| < \pi/2, \quad (18)$$

$$\frac{d\theta}{d\lambda} < 0 \quad \text{for} \quad |\beta| > \pi/2. \quad (19)$$

The sign of $dr/d\lambda$ (or $d\theta/d\lambda$) changes at the turning point where $R = 0$ (or $\Theta = 0$).

Armed with Eqs. (4) to (19), we can trace the trajectories of photons that propagate from the observer at (r_o, θ_o, ϕ_o) back to the initial emitting position $(r_e, \pi/2, \phi_e)$ in the local rest frame of matter moving in the plane of the disc.

¹See the derivation in Ref. [16, 17] for the metric of Kerr black hole. The motion constants could be obtained by replacing the Kerr metric in Karas et al. [16] with the much simple boson star metric. See Fig. 1a in Ref. [16] for a geometric interpretation of the angles involved.

2.3 Disc

In analogy to the standard geometrically thin and optically thick disc around a black hole, such simplified accretion disc now surrounding a massive boson star was first discussed in Ref. [5]. It is assumed that the disc material is in perfect Keplerian motion which gives the following components for the 4-velocity (analogous to the derivation for equatorial disk around Kerr black holes in Ref. [18]):

$$u^t = \sqrt{\frac{2}{2B(r) - rB'(r)}}, \quad (20)$$

$$u^\phi = r^{-\frac{1}{2}} \sqrt{\frac{B'(r)}{2B(r) - rB'(r)}}, \quad (21)$$

$$u^r = 0, \quad (22)$$

$$u^\theta = 0, \quad (23)$$

where $B'(r) = dB(r)/dr$. The rotating velocity of the disc material measured by a static observer is given by

$$v^{(\phi)} = r^{\frac{1}{2}} \sqrt{\frac{B'(r)}{2B(r) - rB'(r)}}. \quad (24)$$

The coordinate-velocity in Eq. (21) is related to angular velocity by $u^\phi = u^t \Omega$.² Note that in the potential of a non-rotating boson star, there are circular orbits for every possible value of the radial coordinate, including those which are inside the boson star [5]. This is clearly different from the black hole case, where the innermost stable circular orbit only extends down to $r = 6r_g$, in the case of a Schwarzschild black hole. As seen from Figure 3, at large radii ($r > 25r_g$), the rotating velocity of the disc surrounding a boson star is the same of that disc surrounding a Schwarzschild black hole. At the innermost part of the disc ($r < 25r_g$), however, differences are not negligible. In the case of a boson star, with decreasing radius, the rotating velocity of the disc increases to a maximum value and then decreases to zero at the star center. In the case of a Schwarzschild black hole, the rotating velocity of the disc increases monotonically until the radius approaches the last stable orbit ($r = 6r_g$). To the view of distant observers, then, this difference results in less Doppler-shifted photons observed in the putative case of a boson star-accretion disc (BS-AD), as compared to the Schwarzschild black hole accretion disc (SchBH-AD).

2.4 Numerical implementation

We shall assume that 1) the disc material is not interacting with the bosons, 2) the distant observer views the disc at some inclination angle θ_o (with $\theta_o = 0^0$ corresponding to a face-on disc). Operationally, we define the distant observer to be located at $r_o = 10^4 r_g$ and $\phi_o = 0^0$. We then integrate the four photon momentum equations from the observer to the accretion disc using motion constants ξ and η . The redshift factor of a photon propagating from the disc to the observer is given by

$$g = \frac{\nu_o}{\nu_e} = \frac{\mathbf{p}_o \cdot \mathbf{u}_o}{\mathbf{p}_e \cdot \mathbf{u}_e}, \quad (25)$$

where ν_o and ν_e are the frequencies of the photon received by the distant observer and the photon emitted in the rest frame of disc material, respectively; \mathbf{p}_o is the photon momentum received by the distant observer and \mathbf{p}_e is the photon momentum in the rest frame of the emitting material. The disc region between r_{out} and r_{in} is divided into 1000×1000 elements ($r_i \rightarrow r_i + dr$, $\phi_i \rightarrow \phi_i + d\phi$). The solid angle subtended at the observer's sky by each element is also calculated by counting the photons impinging onto the element

²Note that there is a typing error in the first of the Eqs. (3) of Ref. [5]: x should be in the denominator.

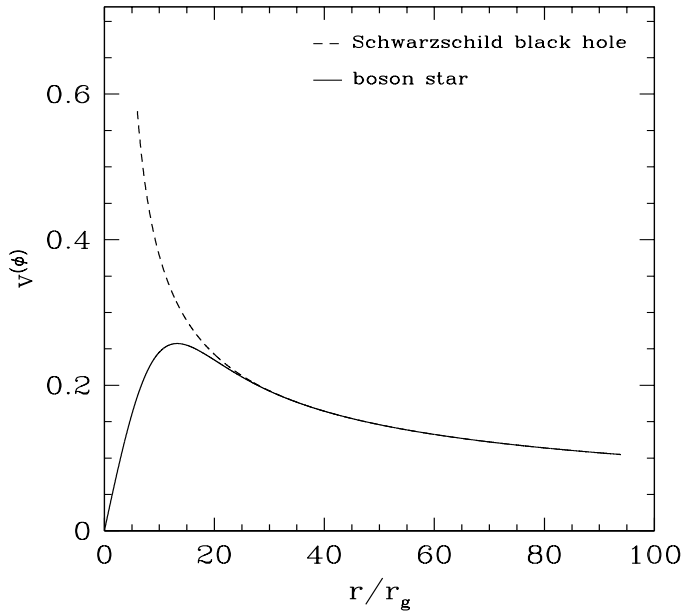


Figure 3: The rotating velocity of the disc material in the view of a static observer as a function a radius (in unit of the gravitation radius $r_g = GM/c^2$). The solid line represents a boson star and the dashed line represents a Schwarzschild black hole.

(we refer the reader to Refs. [17, 19] for further details).

Similar to the case of an accretion disc surrounding a black hole, the disc rotating around a boson star may also be illuminated by some nearby hard X-ray source due to similar mechanism, for example, inverse Compton scattering of soft thermal photons by high energy electrons in the corona above the disc. The fluorescent Fe $K\alpha$ line photons driven by this illumination may directly propagate to distant observers without absorption. We assume, as it is usual, that the X-ray illumination is axisymmetric and the emissivity of Fe $K\alpha$ line only varies with radius as a power law $\epsilon(r) \propto r^{-\alpha}$ in the rest frame of emitting material, where α is the emissivity index. We already know that the viscosity dissipated power per unit area approaches a maximum value at the radius of $\sim 5r_g$ and then rapidly decreases as the accreted material goes into the star center [5]. This is quite different from the case of black hole accretion disc, where the radiation from the region within the marginally stable orbit (in projection) is insignificant.

In order to see the difference between the profiles of the emission lines coming from a BS-AD and from a SchBH-AD, respectively, we consider two cases. In the first one, for a BS-AD, the line is assumed to be emitted from an annulus between $r_{\text{in}} = 6r_g$ and $r_{\text{out}} = 30r_g$. In the second case, the line will be assumed to come from an annulus between $r_{\text{in}} = 2r_g$ and $r_{\text{out}} = 30r_g$. At all times, for a SchBH-AD, the line is assumed to be emitted from annulus between $r_{\text{in}} = 6r_g$ and $r_{\text{out}} = 30r_g$. Physical considerations can be put forward to justify these values of inner and outer limits of the disc. In the case of BS-AD, r_{in} is not chosen to be closer to the center (or 0) because we are adopting a power-law emissivity law which diverges at the star center. *We note, however, that the line emission within $r \leq 2r_g$ would be negligible if the emissivity law is similar to the viscosity dissipated power as a function of radius.* We set $r_{\text{in}} = 6r_g$ in the case of SchBH-AD since the disc only extends to the marginal stable orbit. The line emission from the disc material within the marginal stable orbit is generally assumed negligible, and if this line flux is even

observable, as Reynolds and Begelman [20] have pointed out, it would generally emerge in the extremely red wing of the line profile, what would make the difference between the profiles of Fe $K\alpha$ generated from the BS-AD and from the SchBH-AD that we present in the next Section larger.

The observed line flux distribution is $dF(E_{\text{obs}}) = I(E_{\text{obs}})d\Omega$, where $d\Omega$ is the solid angle subtended by the disc in the observer's sky and $I(E_{\text{obs}})$ is the specific intensity received by the observer. The specific intensity $I(E_{\text{em}})$ of the line emitting in the rest frame of disk material is assumed to be isotropic and monochromatic $I(E_{\text{em}}) = \epsilon(r)\delta(E_{\text{em}} - E_0)$, where E_0 ($= 6.4$ keV for iron $K\alpha$ line) is the energy of the line photons in the rest frame of the emitting material and $gE_{\text{em}} = E_{\text{obs}}$. From the relativistic invariance I_ν/ν^3 (see explanations in Ref. [15], pages 897-902), we have $I(E_{\text{obs}}) = (\nu_o/\nu_e)^3 I(E_{\text{em}}) = g^3 I(E_{\text{em}}) = g^4 \epsilon(r)\delta(E_{\text{obs}} - gE_0)$, and thus the total observed flux distribution of the line is given by

$$F(E_{\text{obs}}) \propto \int_{r_{\text{in}}}^{r_{\text{out}}} \epsilon(r)g^4\delta(E_{\text{obs}} - gE_0)d\Omega_{\text{obs}}, \quad (r_{\text{in}} \leq r \leq r_{\text{out}}). \quad (26)$$

This is what is plotted in the graphs of next Section.

3 Line Profiles

Theoretical emission line profiles produced in the inner region of accretion discs around black holes have been calculated by several authors, see for instance Refs. [21, 22, 23]. The analysis of Section 2 and Section 2.3 has shown that there are two main factors producing differences between the line profiles emitted from the disc extending down within a boson star or the usually considered one accreting around a Schwarzschild black hole:

1. The gravitational potential of a boson star is less deeper than that of a Schwarzschild black hole in the innermost region ($r < 15r_g$).
2. The rotation velocity of the disc around a boson star is smaller than that of the disc around a Schwarzschild black at the inner region with $r < 25r_g$

Figures 4-7 illustrate the line profiles in these two different situations using a completely relativistic calculation with a large range of parameters. Details of the code used can be found in references [17, 19]. These profiles correspond to the inner disc annulus with $r_{\text{in}} = 6r_g$ and $r_{\text{out}} = 30r_g$ (Fig. 4 for $\alpha = 2$ and Fig. 5 for $\alpha = 3$) or with $r_{\text{in}} = 2r_g$ and $r_{\text{out}} = 30r_g$ (Fig. 6 for $\alpha = 2$ and Fig. 7 for $\alpha = 3$) in the case of a BS-AD (solid lines); or with $r_{\text{in}} = 6r_g$ and $r_{\text{out}} = 30r_g$ in the case of a SchBH-AD (dotted lines). All the lines are normalized by their line flux.

These are the main features of our results:

- The lines emitted from the inner region of a BS-AD are somewhat narrower than those emitted from the inner region of a SchBH-AD. The red wing of the lines emitted from the inner region of a BS-AD does not extend to extremely low energy as that from a SchBH-AD because 1) the gravitational shifting of line photons (a factor of $\sqrt{B(r)}$) emitted from the inner region of BS-AD is much less than that from the inner region of SchBH-AD (see Fig. 1 and 2) the Doppler redshifts of line photons in the case of BS-AD is also less than that in the case of SchBH-AD, since the rotating velocity of the inner disc is much smaller in the former case (see also Fig. 3). The high energy blueward extent of the lines emitted from the inner region of BS-AD is determined by the inclination angle of the disc, which is similar to the case of SchBH-AD. However, for the same inclination angle, in the case of BS-AD, the blue horn extends to a larger energy than that in the case of SchBH-AD, since the former case suffers less gravitational redshifts.

- Generally, the line profiles emitted from BS-AD appears to have more peaks than that emitted from SchBH-AD (see Figs. 4-7). For very small inclination angles (e.g. 1^0 , see upper left panel in Figs. 4-7), the line emitted from the inner region of BS-AD is double peaked, and the low energy (more intense) peak is due to the emission from the inner edge where the gravitational shifting is the dominant factor (the transverse Doppler shifting is not large at the inner edge). The line from the inner region of SchBH-AD, on the contrary, tends to a single broad peak (and less intense) with skewed red wings due to much deeper gravitational potential and larger rotating velocity of the disc material near the marginal stable orbit.
- In discs with large inclination angles (e.g. $> 15^0$), the line profiles emitted from the inner region of BS-AD may have more peaks. A typical case with inclination angle $\theta_o = 30^0$ is illustrated in the left bottom panel in Fig. 4: the profile for the inner region of a BS-AD has totally four local maxima compared to the only two local maxima for the case of SchBH-AD. From right to left, the first and the third maximum are due to the line emission in the outer part of the annulus [with $r(v \sim v_{\max})$]. There are small displacements between these two maxima and the corresponding two maxima in the case of SchBH-AD. The second and the fourth maximum are due to the line emission from the inner part of the annulus [with $r(v \lesssim v_{\max})$]. There are no such two corresponding peaks in the case of SchBH-AD because combined effects of the much deeper gravitational potential of the black hole and the larger disc rotation velocity shifts the line photons to lower or higher energy and smooth the line profile to the skewed one.

4 Concluding remarks

Observations of the central regions of active galaxies already exist. For some of them, the Iron $K\alpha$ profile could be measured and interesting conclusions can be already drawn. For instance, given the observations of MCG-6-30-15, in which the red wing of the Fe $K\alpha$ extends down to energy of 2-3 keV [24], the computations of this paper have clearly shown that the central object in this galaxy cannot be a non-rotating massive boson star. It would be of interest, though, to study more complicated cases of accretion discs, particularly those around rotating boson stars. The observational data will be very much improved with forthcoming technologies. The NASA Constellation-X [25] mission, to be launched in 2008, is optimized to study the iron $K\alpha$ line features and will determine the black hole mass and spin for a large number of systems. A detection of several peaks at lower energies, or of intense double peaks in faced on galaxies could be an impressive indication of a boson star nucleus. More importantly, this paper gives a new way to examine an interesting theoretical construct with real astrophysical data, helping to elevate the boson star concept to a falsifiable level.

Acknowledgments

YL thanks the hospitality of the Astrophysical Sciences Department of Princeton University. DFT acknowledges support from Fundaci3n Antorchas, CONICET, and the Physics Department of Princeton University.

References

- [1] Rees, M. J. 1984, ARAA, 22, 471
- [2] Kormendy, J., and Reihstone, D. 1995, ARAA, 33, 581

- [3] Magorrian, J., et al. 1998, *AJ*, 115, 2285
- [4] Torres, D. F., Capozziello, S. and Lambiase, G. 2000, *Phys. Rev. D* **62**, 104012 (2000) [arXiv:astro-ph/0004064].
- [5] Torres, D. F. 2002, *Nucl. Phys. B* **626**, 377 [arXiv:hep-ph/0201154].
- [6] Another possible non-baryonic center, the neutrino ball, was presented by Viollier R. D., Trautmann D., Tupper G. B. 1993, *Phys. Lett. B* 306, 79, and later by Bilic N., Munyaneza F. and Viollier R. D. 1999, *Phys. Rev. D* 59, 024003. In the neutrino ball scenario the central object is an extended one, and gravitational effects are much more weaker. This translates into observational effects related with star orbits, see Munyaneza F., and Viollier, R. D. 2002, *ApJ* 564, 247.
- [7] Tanaka, Y., et al. 1995, *Nature*, 375, 659
- [8] Fabian, A. C., Nandra, K., Reynolds, C. S., Brandt, W. N., Otani, C., Tanaka, Y., Inoue, H., and Iwasawa, K. 1995, *MNRAS*, 277, L11
- [9] Lee, T. D., and Pang, Y. 1992, *Phys. Rep.* 221, 251; Liddle, A. R., and Madsen, M. S. 1992, *Int. J. Mod. Phys. D* 1, 101; Mielke, E. W., and Schunck, F. E. 1999, *Proceedings of the 8th Marcel Grossmann meeting in Jerusalem* (World Scientific Publ., Singapore, p.1607), gr-qc/9801063.
- [10] Torres D. F. 1997, *Phys. Rev. D* **56**, 3478 [arXiv:gr-qc/9704006]; Torres, D. F., Liddle, A. R., and Schunck, F. E. 1998, *Phys. Rev. D* **57**, 4821 [arXiv:gr-qc/9710048]; Torres, D. F., Schunck, F. E., and Liddle, A. R. 1998, *Class. Quant. Grav.* **15**, 3701 (1998) [arXiv:gr-qc/9803094].
- [11] Ruffini, R., and Bonazzola, S. 1969, *Phys. Rev.* 187, 1767
- [12] Kaup, D. J. 1968, *Phys. Rev.* 172, 1331
- [13] Colpi, M., Shapiro, S. L., and Wasserman, I. 1986, *Phys. Rev. Lett.* 57, 2485
- [14] Chandrasekhar, S. 1983, *The Mathematical Theory of Black Holes*, Oxford University Press, Oxford
- [15] Misner, C. W., Thorne, K. S., and Wheeler, J. A. 1973, *Gravitation* (San Fransisco: W. H. Freeman & Co.)
- [16] Karas, V., Vokrouhlický, D., and Polnarev, A. G., 1992, *MNRAS*, 259, 569
- [17] Lu, Y., and Yu, Q. 2001, *ApJ*, 561, 660
- [18] J. M. Bardeen, W. H. Press, and S. A. Teukolsky, *ApJ* **178**, 347 (1972).
- [19] Yu, Q., and Lu, Y. 2000, *MNRAS*, 311, 161
- [20] Reynolds, C. S., and Begelman, M. C. 1997, *ApJ*, 488, 109
- [21] Fabian, A. C., Rees, M. J., Stella, L., and White, N. E. 1989, *MNRAS*, 238, 729
- [22] Laor, A. 1991, *ApJ*, 376, 90
- [23] Fanton, C., Calvani, M., de Felice, F., and Cadez, A. 1997, *PASJ*, 49, 159
- [24] Wilms, J., Reynolds, C. S., Begelman, M. C., Reeves, J., Molendi, S., Staubert, R., and Kendziorra, E. 2001, *MNRAS*, 328, L27
- [25] Constellation-X web page: <http://constellation.gsfc.nasa.gov/>

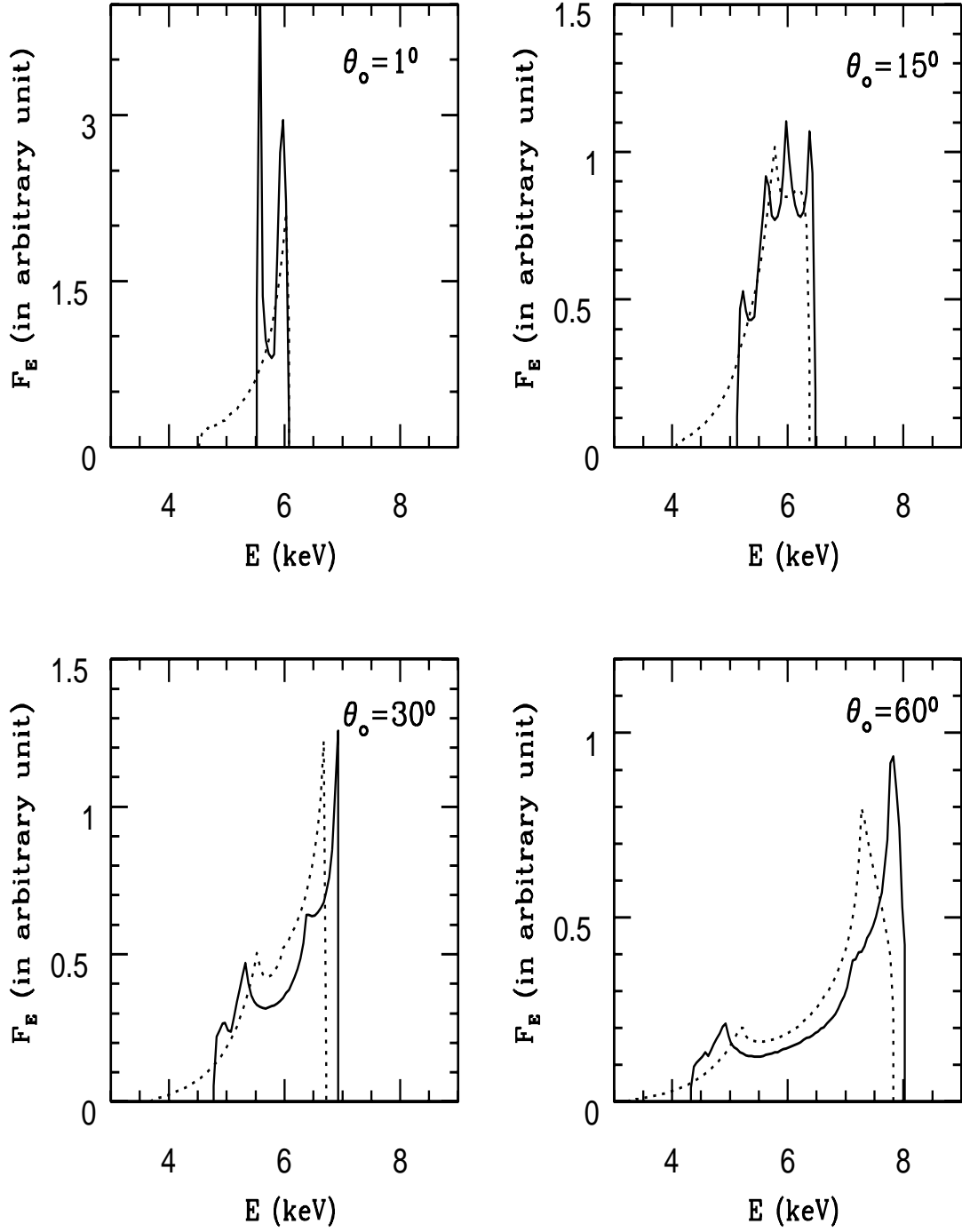


Figure 4: Line profiles computed using complete relativistic method as described in the text. The line emitting region for all the cases is fixed to be the annulus with $r_{\text{in}} = 6r_g$ and $r_{\text{out}} = 30r_g$. The line emissivity law is set to be $\epsilon \propto r^{-2}$ and the inclination angles are labeled in each panel. The solid lines and dashed lines represent the profiles of lines from boson star-accretion disc and from Schwarzschild black hole-accretion disc, respectively.

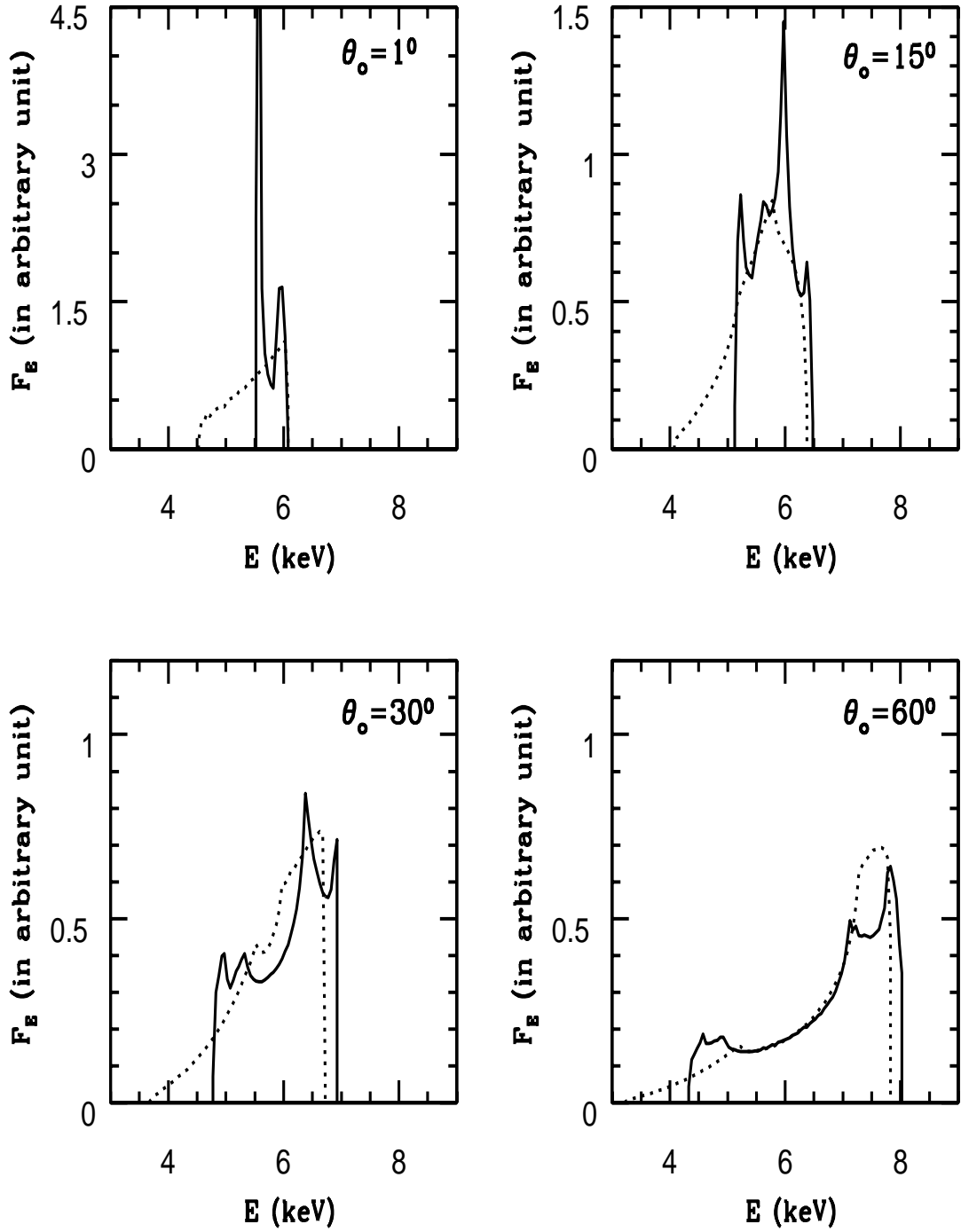


Figure 5: Same as Fig. 4, but adopt a different emissivity law of $\epsilon \propto r^{-3}$.

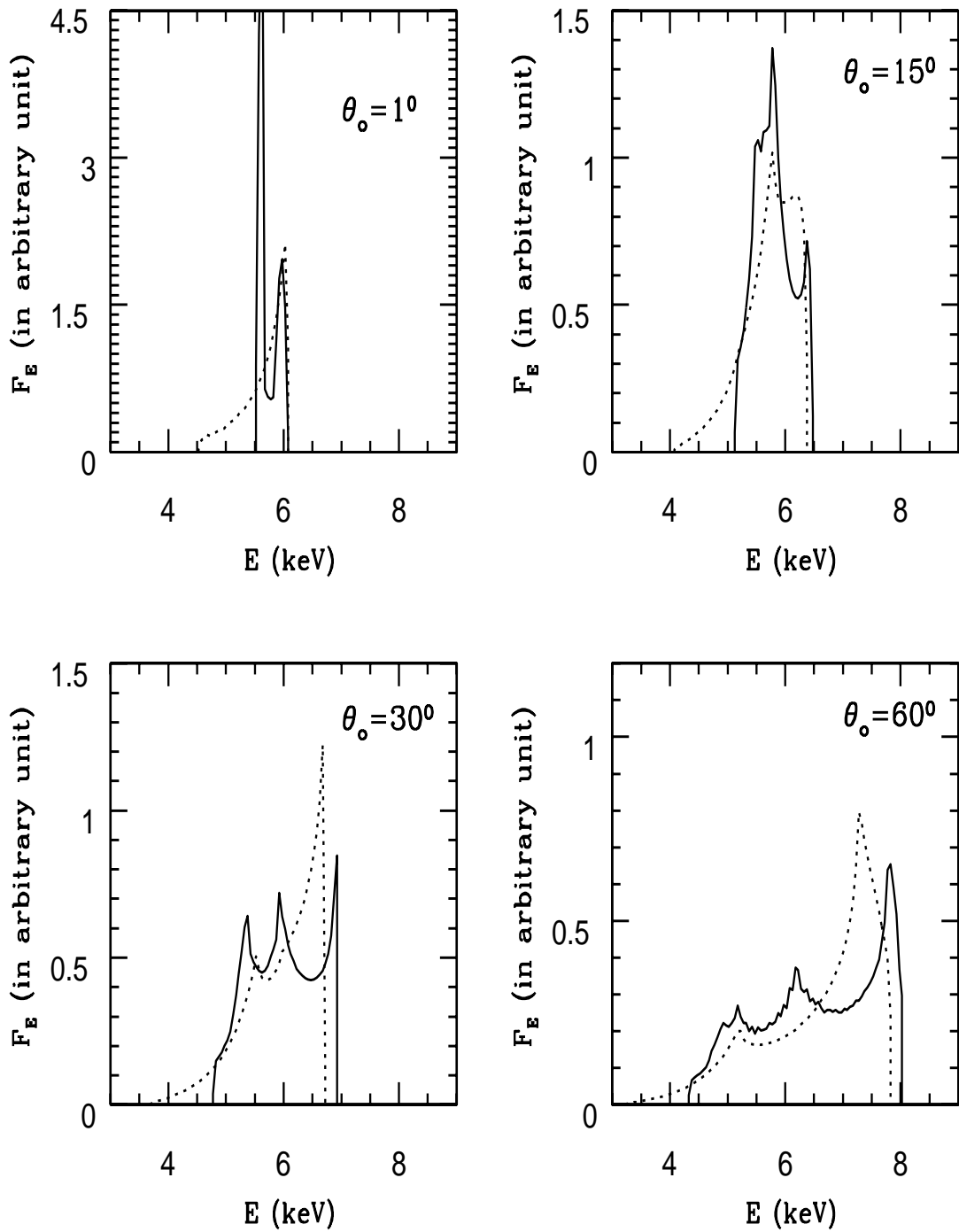


Figure 6: Same as Fig. 4, but adopt a different inner radius $r_{\text{in}} = 2r_g$ of the line emitting annulus for the case of the boson star-accretion disc.

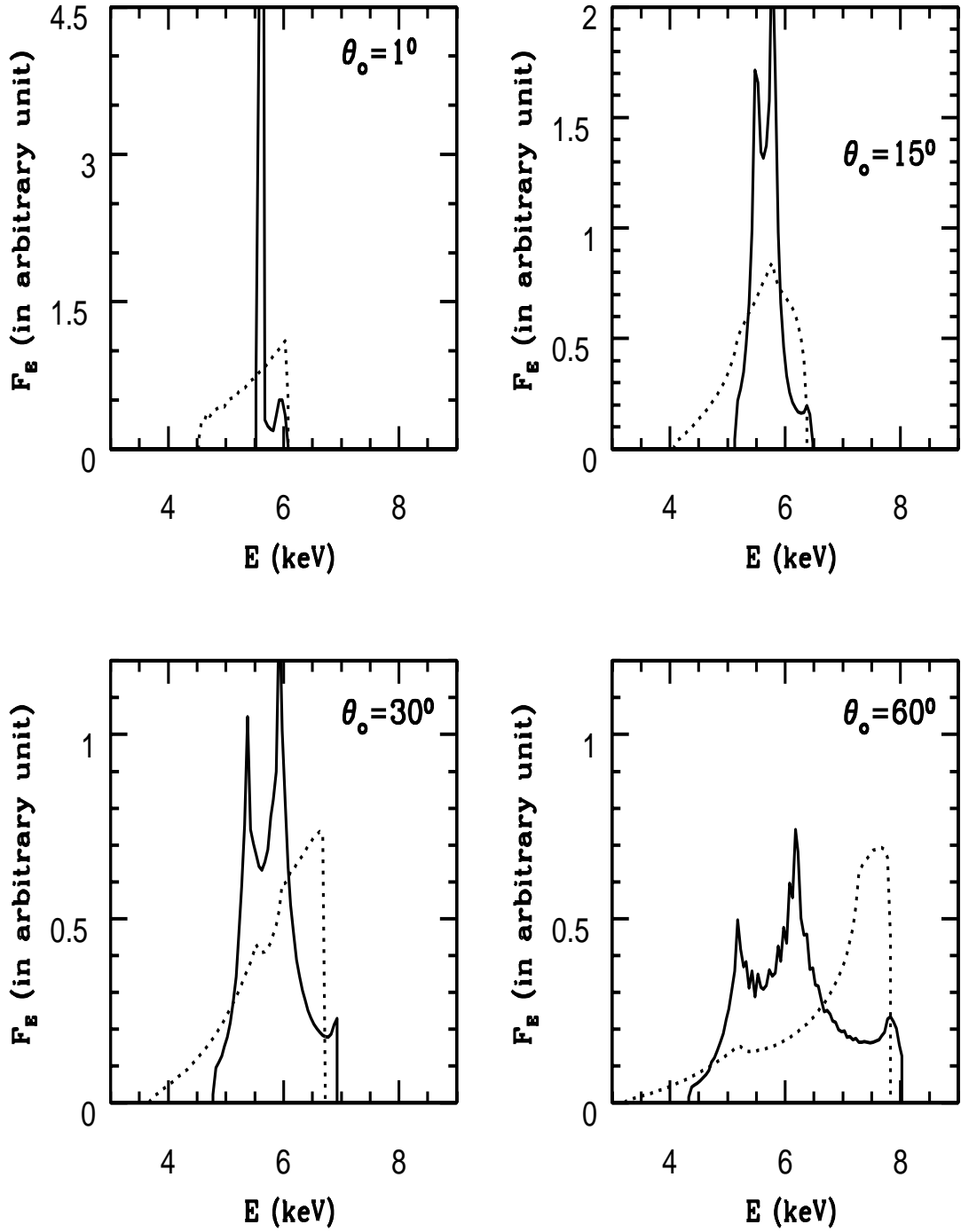


Figure 7: Same as Fig. 6, but adopt a different emissivity law of $\epsilon \propto r^{-3}$.